Dielectric relaxation in PAN/EC/PC (poly-(acrylonitrile)/ethylene carbonate/propylene carbonate) mixtures

1999 J. Phys.: Condens. Matter 11 10285

(http://iopscience.iop.org/0953-8984/11/50/321)

J. Phys.: Condens. Matter **11** (1999) 10285–10295. Printed in the UK PII: S0953-8984(99)05101-2

Dielectric relaxation in PAN/EC/PC (poly-(acrylonitrile)/ethylene carbonate/propylene carbonate) mixtures

H Eliasson†, B-E Mellander† and L Sjögren‡

† Fysik och Teknisk Fysik, Göteborgs Universitet och Chalmers Tekniska Högskola, SE-412 96 Göteborg, Sweden

‡ Institutionen för Fysik och Teknisk Fysik, Göteborgs Universitet, SE-412 96 Göteborg, Sweden

Received 9 June 1999

Abstract. Dielectric measurements have been performed on a series of samples consisting of poly-(acrylonitrile) (PAN) mixed with the plasticizers ethylene carbonate (EC) and propylene carbonate (PC) in various proportions. The spectra obtained show characteristic features such as a linear $\ln(\omega)$ variation, a horizontal inflection point and double minima, which are predicted within the A_4-scenario of the mode-coupling theory. We find very good agreement with the theoretical results in the relevant frequency range. The experimental spectra are found to satisfy a scaling behaviour, and the resulting master curves are in good agreement with the theoretical predictions.

1. Introduction

The dielectric and mechanical properties of polymers have been a topic of great interest for a long time [1,2]. The reason for studying these materials has not only been to gain insight into the relaxation mechanisms of the individual polymer molecules, but also to study the liquid–glass transition, since many polymers are ideal glass formers. However, due to the complexity of the systems studied, there has still not emerged any generally accepted theory capable of describing all phenomena occurring in these materials. In fact, most models proposed build upon some more or less crude assumptions. Furthermore, the analysis of experimental data is usually performed in terms of empirical or quasi-empirical models such as the Kolrausch–Williams–Watts (KWW) formula [3,4], the Havriliak–Negami (HN) function [5], the Vogel–Tammann–Fulcher (VTF) equation [6–8] and other models. Even though a large class of spectra can be successfully analysed with the KWW or HN formulae in the α- and β-relaxation regions, there exist spectra with a more complicated $1/f$ noise character [9–16], where these simple empirical formulae do not apply.

During recent years a microscopic approach to slow relaxations in glassy systems has been proposed. This so-called mode-coupling theory (MCT), has brought to light many unexpected and non-trivial results, and has partly led to a completely new way in which to analyse experimentally obtained data. In particular, it was possible to successfully analyse the more complex spectra mentioned above [17–20] in addition to the simpler scenarios with a single α-peak. In the original formulation, one starts from Newton's equations for the motion of particles in a monatomic simple liquid of spherical molecules. Using the so-called

0953-8984/99/5010285+11$30.00

Zwanzig–Mori formalism [21] an expression for the density autocorrelation function $\phi(q, z)$ is obtained as

$$\phi(q, z) = -1/\left[z - \Omega^2(q)/(z + M(q, z))\right] \tag{1}$$

where z is a complex frequency, q the wave-vector modulus, $\Omega(q) = q^2/\beta m S(q)$ a characteristic frequency for liquid dynamics and $M(q, z)$ a generalized longitudinal viscosity or memory function. Here $\beta = 1/k_B T$ and $S(q)$ denotes the static structure factor. An exact evaluation of this memory function is not possible, so it has to be approximated in some way. In MCT, this is done by first observing that it is possible to split it into two parts, $M(q, z) = i\nu(q) + \Omega^2(q)m(q, z)$, where the first term describes fast, uncorrelated, binary collision events and the second corresponds to collective events with repeated correlated collisions. For the latter term one performs a mode-coupling approximation [22, 23] which leads to the expression

$$m(q, t) = \sum_{k+p=q} V(q, k, p)\phi(k, t)\phi(p, t) \tag{2}$$

where the coupling constants V are given in terms of the static structure factor $S(q)$.

From these expressions, singularities will appear in a quite subtle way, due to an ergodic–non-ergodic transition at a certain temperature T_c, characterized by $\phi(q, t \to \infty) = f(q) > 0$. If the coupling constants, V, for a particular system are considered to be coordinates in a parameter space, then the set of singularities will make up a hypersurface marking the limit between liquid and ideal glassy states. The singularities are of the so-called cuspoid type [24, 25]. Close to a singularity the above equations can be solved asymptotically. Specifically, the factorization property

$$\phi(q, t) = f^c(q) + h(q)G(t) \tag{3}$$

is found to hold in a time region $t_0 \ll t \ll \tau_\alpha$, where t_0 is a microscopic time and τ_α the α-relaxation time. This time window is referred to as the β-relaxation region. The factor $f^c(q)$ is the value of the long-time limit of $\phi(q, t)$ at the singularity and $h(q)$ is an amplitude. Because of this factorization, the complete relaxation pattern in the β-relaxation region is described by the function $G(t)$ only. This implies a universal relaxation scenario, since a similar relation holds for any relaxation function $\phi_{XY}(q, t)$, i.e. $\phi_{XY}(q, t) = f^c_{XY}(q) + h_{XY}(q)G(z)$, where X and Y represent variables with a non-zero overlap with the density. In particular, for the dielectric function $\epsilon(z)$ one finds [17]

$$\epsilon(z) = f_\epsilon + h_\epsilon z G(z). \tag{4}$$

The master function $G(t)$ obeys the equation

$$\begin{aligned} -\frac{\delta_0}{z} + \delta_1 G(z) + zG^2(z) + (1 + \delta_2)\mathrm{LT}\left[G^2(t)\right](z) \\ - \gamma_3 z^2 G^3(z) + (\delta_3 + \gamma_3)\mathrm{LT}\left[G^3(t)\right](z) \\ + \gamma_4 z^3 G^4(z) + (\delta_4 + \gamma_4)\mathrm{LT}\left[G^4(t)\right](z) + \cdots \\ \cdots + (-1)^k \gamma_k z^{k-1} G^k(z) + (\delta_k + \gamma_k)\mathrm{LT}\left[G^k(t)\right](z) + \cdots = 0 \end{aligned} \tag{5}$$

where LT denotes the Laplace transform:

$$\mathrm{LT}\left[G(t)\right](z) = \mathrm{i}\int_0^\infty G(t)\mathrm{e}^{\mathrm{i}zt}\,\mathrm{d}t \tag{6}$$

and the parameters δ_k and γ_k are given as certain integrals over the coupling constants $V(q, kp)$ in equation (2). Depending on the behaviour of the coefficients in equation (5), the singularities discussed above are classified in the following manner: at the singularity, $\delta_0 = \delta_1 = 0$, and if

$\delta_2 \neq 0$, an A_2- or Whitney-fold singularity is encountered. If also $\delta_2 = 0$ but $\delta_3 \neq 0$, we have an A_3- or Whitney-cusp singularity, and so on.

A large number of experimental data have been analysed in terms of an A_2-singularity [26, 27]. The function $G(z)$ is in this case given by a simple scaling law, and its shape determined by two power laws. The purpose of the present paper is to study some aspects of the higher-order scenarios where $G(t)$ is given by elliptic functions, yielding a more complex relaxation pattern. In particular we will find that experimental data on PAN show some of the characteristic features of an A_4- or swallowtail singularity, and some of the intricate scaling predictions of the theory will be verified.

1.1. The cusp scenarios

For the singularities A_k, with $k \geqslant 3$, $G(t)$ in equation (5) has the solution [28]

$$G(t) = \rho^2 f\left[\ln\left(\frac{t}{t_1}\right)\right] \tag{7}$$

where $\rho = \left[2\pi^2/3\mu_k(k-2)^2\right]^{1/2(k-2)}$. The coefficient μ_k is the negative value of δ_k at the singularity. The function f satisfies the differential equation

$$\left(\frac{\mathrm{d}f}{\mathrm{d}y}\right)^2 = \frac{4}{(k-2)^2} f^k(y) - g_2 f^{k-2}(y) - \cdots - g_{k-1} f(y) - g_k \tag{8}$$

where $y = \ln(t/t_1)$ and t_1 is a microscopic time. Here $g_\ell = 4\delta_{k-\ell}/\mu_k(k-2)^2\rho^{2\ell}$ are mathematical control parameters which all vanish at the singularity. We can transform equation (7) into the frequency domain, which in leading order yields

$$G(\omega) = -\frac{1}{\omega}\rho^2\left\{f\left[\ln\left(\frac{1}{\omega t_1}\right)\right] + \mathrm{i}\frac{\pi}{2} f'\left[\ln\left(\frac{1}{\omega t_1}\right)\right]\right\} \tag{9}$$

where $f'(y) = \mathrm{d}f/\mathrm{d}y$. Then the dielectric function $\epsilon(\omega) = \epsilon'(\omega) + \mathrm{i}\epsilon''(\omega)$ is given by

$$\epsilon'(\omega) = f_\epsilon - \epsilon_c f(\ln(1/\omega t_1)) \tag{10a}$$

$$\epsilon''(\omega) = -\frac{\pi}{2}\epsilon_c f'(\ln(1/\omega t_1)) \tag{10b}$$

where $\epsilon_c = h_\epsilon \rho^2$ and f_ϵ will be treated as fitting parameters. The different singularities A_k all exhibit their own quite distinctive signatures. In the A_4-case, which is the one relevant here, the imaginary part of the dielectric susceptibility is characterized by e.g. frequency-independent regions, double minima, inflection points and regions linear in $\ln(\omega)$, as will be seen in figures 3, 4 and 5, later.

Equation (8) can be rewritten into an integral form and for the A_4-case one obtains the elliptic integral [18]

$$y = \int_f^\infty \frac{\mathrm{d}s}{\sqrt{s^4 - g_2 s^2 - g_3 s - g_4}}. \tag{11}$$

The function $f(y; g_2, g_3, g_4)$ is homogeneous since

$$f(y; g_2, g_3, g_4) = sf(sy; s^{-2}g_2, s^{-3}g_3, s^{-4}g_4) \tag{12}$$

and by putting $s = |g_4/3|^{1/4} = 1/y_4$ the real and imaginary parts of the dielectric function can be written as

$$\epsilon'(\omega) = f_\epsilon - \epsilon_c f(\ln(1/\omega t_1); g_2, g_3, g_4) = f_\epsilon - c_4' f(u; \pm 6r^{1/2}, \pm 8p^{1/4}, \pm 3) \tag{13a}$$

$$\epsilon''(\omega) = -\frac{\pi}{2}\epsilon_c f'(\ln(1/\omega t_1); g_2, g_3, g_4) = -c_4'' f'(u; \pm 6r^{1/2}, \pm 8p^{1/4}, \pm 3) \tag{13b}$$

where $u = \ln(1/\omega t_1)/y_4$, $r = \left|g_2^2/12g_4\right|$ and $p = \left|27g_3^4/4096g_4^3\right|$. Here r and p have been defined such that $r = p = 1$ corresponds to the cusp points in figure 2—see later. The scaling parameters c_4', c_4'' and $y_4 = 1/s$ are predicted to have the following temperature dependence:

$$c_4' \propto \left|\frac{T - T_0}{T_0}\right|^{1/4} \tag{14a}$$

$$c_4'' \propto \left|\frac{T - T_0}{T_0}\right|^{1/2} \tag{14b}$$

$$\frac{1}{y_4} \propto \left|\frac{T - T_0}{T_0}\right|^{1/4} \tag{14c}$$

where T_0 is the location of the swallowtail singularity, i.e. the temperature where g_2, g_3 and g_4 all vanish. If these parameters are regarded as coordinates in a three-dimensional parameter space, then this space will contain scaling lines where the parameters r and p are constant. If a set of dielectric spectra yields parameter points (g_2, g_3, g_4) which lie on such a scaling line, it must be possible to rescale these spectra according to equations (13) so that they fall on a common master curve. The scaling amplitudes obtained should then have the temperature dependence given by equations (14). A consistency check of these relations can be obtained from the extracted values of c_4', c_4'' and y_4, since

$$s = \frac{1}{y_4} = \left|\frac{g_4}{3}\right|^{1/4} = \frac{2c_4''}{\pi c_4'}. \tag{15}$$

It is impossible to analytically evaluate $f(y)$ from equation (8) for $k = 4$. Instead, we proceeded by numerically calculating the integral in equation (11) for given values of f. With $y = \ln(1/\omega t_1)$ it was in this way possible to generate sets of curves for $f[\ln(1/\omega t_1)]$. The dielectric function was then easily obtained from equations (13). To fit the experimental curves to these functions, we started by noting that by using equation (8) with $k = 4$, it is possible to eliminate ω from equations (13) [19], so one can express ϵ''^2 as a function of ϵ'. The relation between these turns out to be a fourth-order polynomial and it is thus possible to use ordinary linear least-squares fitting algorithms to find all parameters involved, i.e. f_ϵ, ϵ_c, g_2, g_3 and g_4.

2. Experimental section

The samples were prepared by mixing 1.5 g of ethylene carbonate (EC, supplied by Fluka) with 0.1 g of propylene carbonate (PC, Aldrich Chemical Company Incorporated, UK) over a hot plate held at 90 °C. 0.4 g of poly(acrylonitrile) (PAN, Aldrich) was then added and the mixture was stirred at the same temperature for an hour. The glass vessel containing the mixture was kept sealed during the preparation. Still at the same temperature, the sealing was removed so that the PC and EC were free to evaporate. Samples were then taken from the resulting gel at regular intervals, first every 10 minutes for the first 30 minutes and then every 5 minutes until the gel had hardened; see table 1. The samples were all pressed between two glass plates into films with thicknesses around 0.15 mm.

The dielectric measurements were performed with a Hewlett-Packard 4291A RF Impedance Analyzer having a frequency range of 1 MHz to 1.8 GHz. The sample cell was a Novocontrol BDS2100 equipped with an RF extension line from Novocontrol. The temperature was regulated by letting water from a thermostatic bath flow through a cylindrical metal container surrounding the sample cell. The temperature was measured with a chromel–alumel thermocouple.

Table 1. Preparation of PAN/EC/PC samples.

Sample No	Evaporation time (min)
1	0
2	10
3	20
4	30
5	35
6	40
7	50
8	55
9	60
10	65
11	70
12	75
13	80
14	85

3. Results and discussion

Before any theoretical analysis of the data was attempted, the dc conductivity contribution to the imaginary part of the dielectric function was subtracted. A typical plot of the dc conductivity for one of the samples versus inverse temperature is seen in figure 1. A distinct jump in the conductivity is detected at around 30 °C. This is probably due to the crystallization of EC. Worth noting also is that the conductivity is fairly high (around 10^{-5} S cm^{-1}).

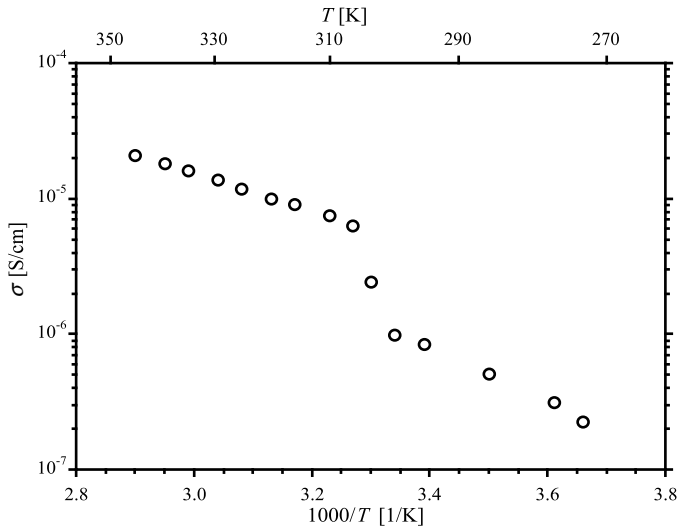

Figure 1. DC conductivity plotted as a function of inverse temperature.

Figure 2 shows the positions in the g_2–g_3–g_4 parameter space of all the measured spectra. Because of the homogeneity properties of the elliptic function $f(y)$, it is possible to completely specify this three-dimensional space with the three surfaces defined by the cuts with the planes $g_2 = 1$, $g_2 = 0$ and $g_2 = -1$. The full lines are the crossover surfaces between ideal glassy and liquid states and are the sets of all A_2-singularities. The dotted part of the 'swallowtail'

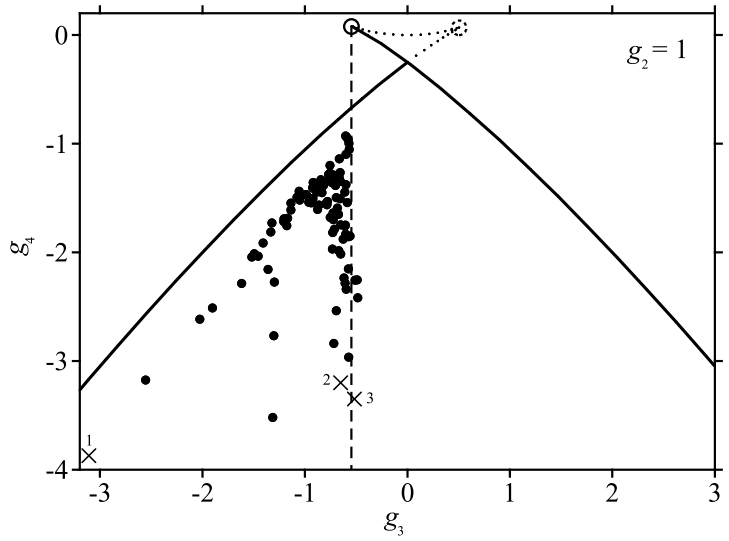

Figure 2. A cut of the g_2–g_3–g_4 space with the plane $g_2 = 1$. The open circles indicate the positions of the cusp points and the black circles are the positions of the measured spectra in this parameter space. The crosses with numbers refer to the spectra shown in figures 3, 4 and 5.

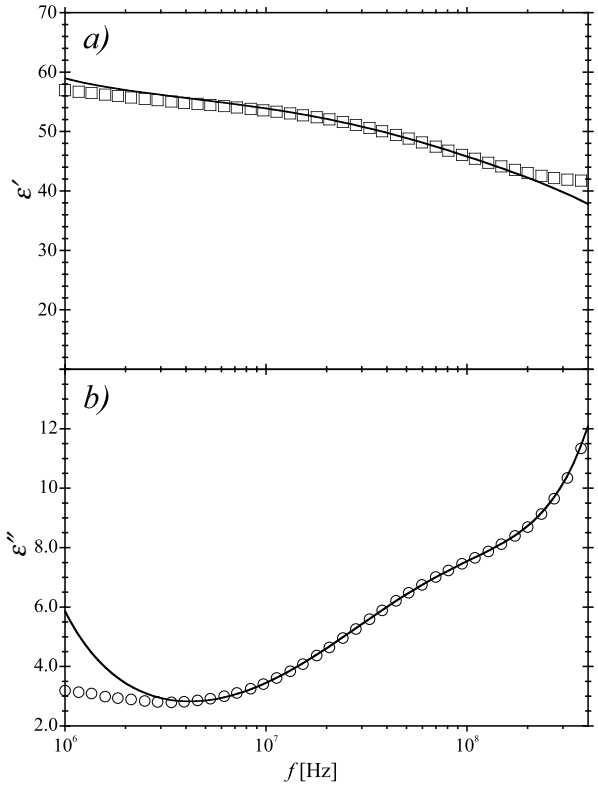

Figure 3. Real (a) and imaginary (b) parts of the dielectric function plotted as functions of frequency for sample 1 at 338 K, corresponding to point 1 in figure 2. The full lines are fits to equations (10).

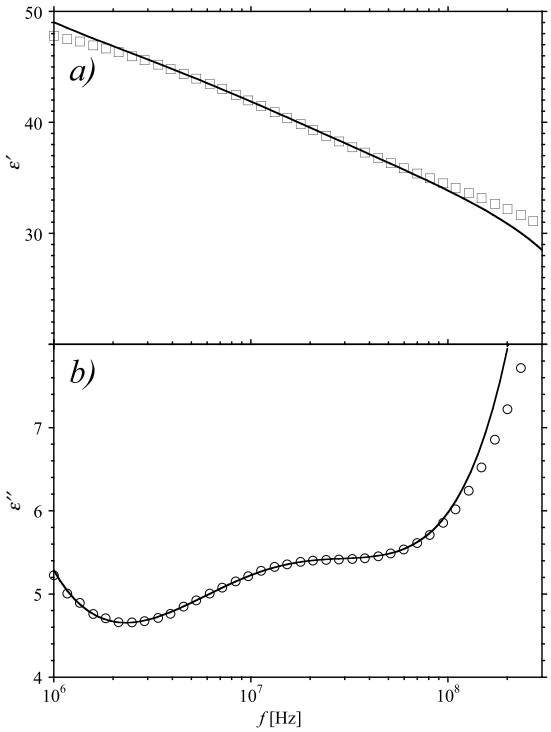

Figure 4. Real (a) and imaginary (b) parts of the dielectric function plotted as functions of frequency for sample 2 at 297 K, corresponding to point 2 in figure 2. The full lines are fits to equations (10).

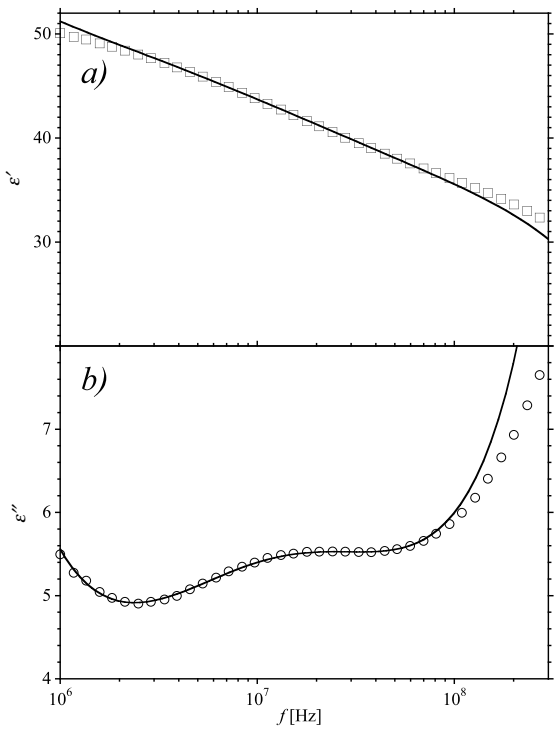

Figure 5. Real (a) and imaginary (b) parts of the dielectric function plotted as functions of frequency for sample 4 at 294 K, corresponding to point 3 in figure 2. The full lines are fits to equations (10).

corresponds to an unphysical situation. The dashed straight line, which starts at the left cusp point, contains the set of parameter points for which the spectra exhibit a horizontal inflection point. Two distinct sets of experimental points can be identified in this plot, one set that follows the bifurcation surface on the left represented by the full line, and one set of points that lie on a line parallel to and close to the dashed line of horizontal inflection points.

In figures 3, 4 and 5, the real, $\epsilon'(\omega)$, and imaginary, $\epsilon''(\omega)$, parts of the dielectric function are plotted as functions of frequency for three typical spectra taken from the sets mentioned above. These spectra show the low-frequency wing of a peak centred around 10^9 Hz followed by a broad structure with either (a) a linear part in $\ln(\omega)$ (corresponding to the cross labelled '1' in figure 2 and the spectra of which are shown in figure 3), (b) a plateau followed by a minimum (corresponding to the cross with label '2' in figure 2 and the spectra in figure 4) or (c) the tendency of a double minimum and a maximum in between (labelled '3' in figure 2 and the spectra in figure 5). For lower frequencies, $\epsilon''(\omega)$ starts to increase and eventually we expect an α-peak outside the experimental window. All these features are characteristic for an A_4-scenario [18], and the full lines are the best fits to theoretical curves as described above. Clearly these spectra are not easily fitted with conventional KWW or HN models.

The r- and p-parameters were calculated from the curve fits for all the measured spectra. By comparing these values it was possible to distinguish a set of a few spectra for which these parameters had approximately constant values. According to the theory it should then be possible to rescale these spectra to fall on a master curve which can be calculated from equations (13). This is shown in figure 6 where the real and imaginary parts of the dielectric

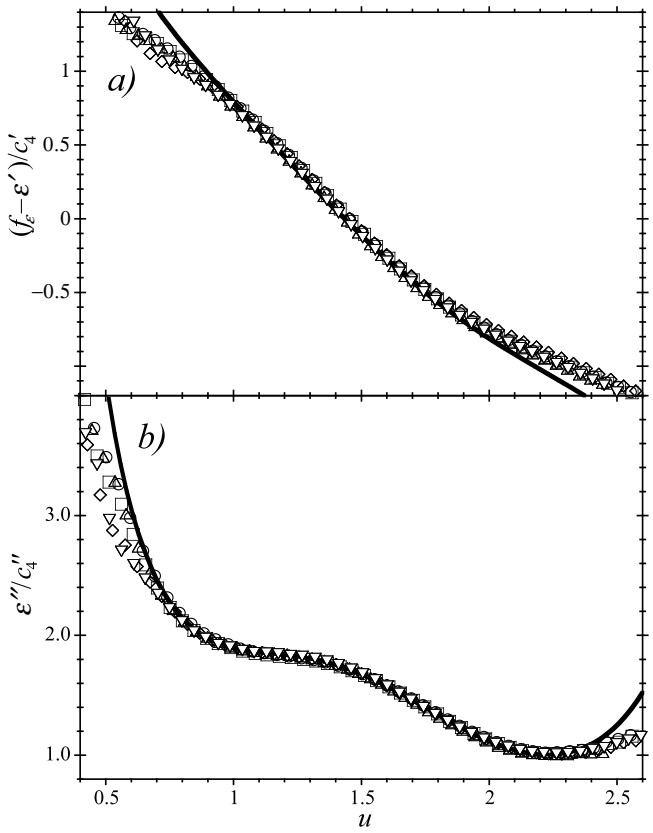

Figure 6. Real (a) and imaginary (b) parts of the rescaled dielectric function for five different spectra plotted as functions of $u = -\ln(\omega t_1)/y_4$; see the text. The full lines are the calculated master curves with $r = 0.064$ and $p = 0.0011$. Circles: sample 2 at 323 K; squares: sample 5 at 324 K; diamonds: sample 13 at 332 K; up-pointing triangles: sample 5 at 319 K; down-pointing triangles: sample 8 at 335 K; see table 1.

function are rescaled and plotted as functions of $u = \ln(1/\omega t_1)/y_4$. Clearly the experimental curves fall on a master curve when shifted in an appropriate way, and this master curve agrees with the theoretical curve given by the full line. On the high-frequency side or for low u-values, the data start to deviate from the scaling behaviour and we see some discrepancies with respect to the theoretical master curves. There is also a systematic deviation for low frequencies or large u-values, but in this region the results are very sensitive to the value of the conductivity used to subtract the low-frequency $1/\omega$ behaviour.

From figure 6, the scaling parameters c_4', c_4'' and y_4 can be extracted. The predicted temperature dependences of these parameters are given by equations (14). In our case, however, there are too few points available and the temperature range that could be investigated was too limited, making it impossible to fully test these predictions. This is illustrated in figure 7, where c_4', c_4'' and $1/y_4$ together with the fitting parameter g_4 are plotted as functions of temperature. The full lines are the best fits to equations (14). In these fits, the temperature T_0 was fixed to a value of 235 K, determined from a straight-line fit of g_4 as a function of temperature in figure 7(a). This temperature value is far below the lowest accessible temperature of 320 K.

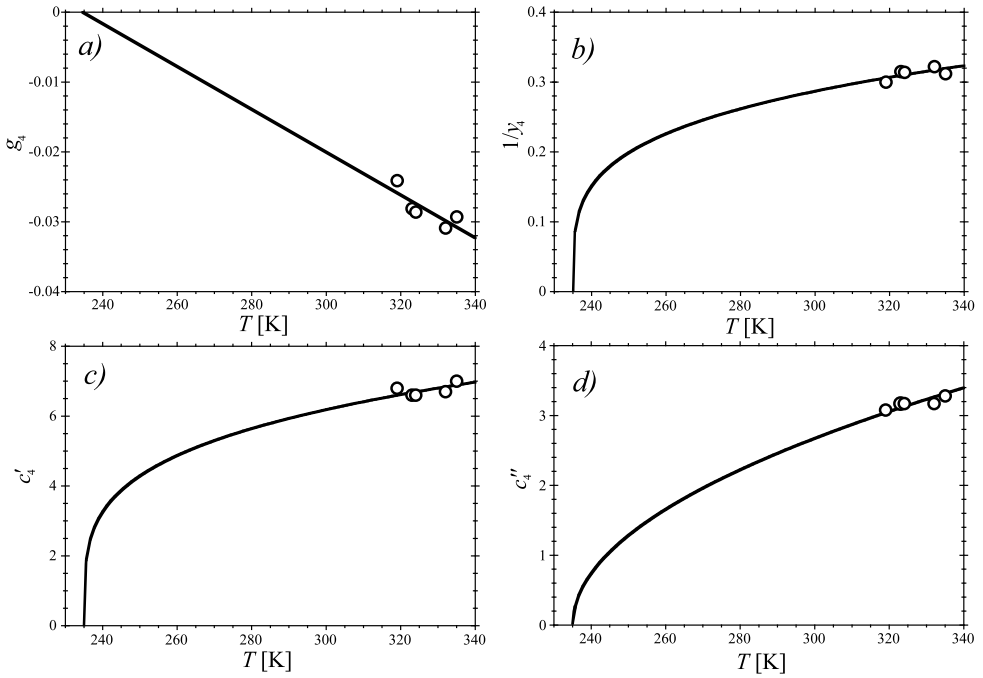

Figure 7. Plots of the different scaling parameters versus temperature; see the text. (a) g_4. The full line is the best fit to a straight line, yielding $T_0 = 235$ K. (b) The scaling parameter $1/y_4$. The full line is the best fit to the function $1/y_4 = k_1(T - 235)^{1/4}$. (c) The scaling parameter c_4'. The full line is the best fit to $c_4' = k_2(T - 235)^{1/4}$. (d) The scaling parameter c_4'' where the full line is the best fit to the equation $c_4'' = k_3(T - 235)^{1/2}$.

According to the discussion in the introduction, the parameters shown in figure 7 are interrelated according to equation (15). This prediction is tested in figure 8. The good correspondence found between the experimentally determined scaling parameters c_4' and c_4'' indicates that the asymptotic expressions for both ϵ' and ϵ'' are valid in the present case.

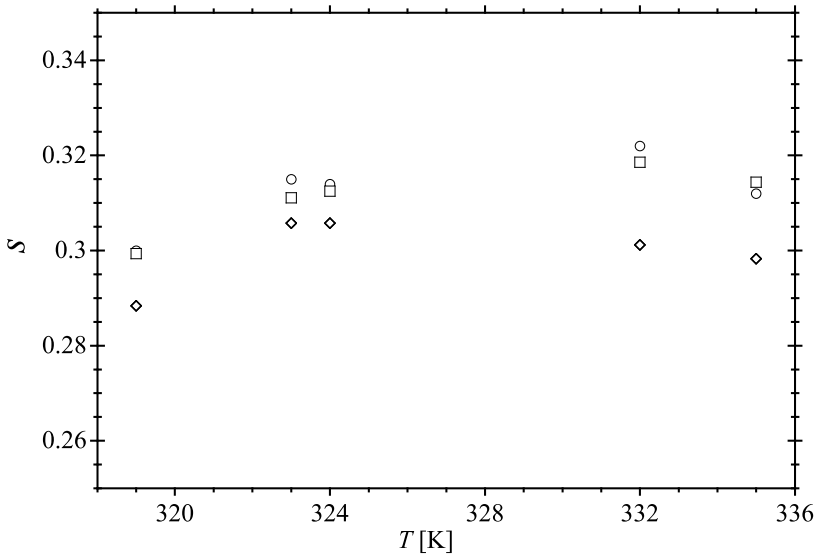

Figure 8. Plots of the recalculated scaling parameters from figure 7; see the text. Circles: $s = 1/y_4$; squares: $s = |g_4/3|^{1/4}$; diamonds: $s = 2c_4''/(\pi c_4')$.

4. Conclusions

In accordance with other studies [17–20], we find that a higher-order scenario of the MCT can be used to explain the relaxation patterns in amorphous and semi-crystalline polymers quite well. That the system under study is rather far away from the A_4-singularity is demonstrated by the fact that the frequency region over which there is correspondence between theory and experiment is fairly small, in this case only around two decades. The asymptotic nature of the MCT functions predicts that this frequency region will expand as the temperature is decreased towards the critical temperature T_0. A crucial test of the MCT predictions is to find out whether the scaling relations in equations (14) are fulfilled. In the present case, this was not possible due to the limited temperature interval available. However, a set of spectra were found which could be rescaled onto a master curve, and the shape of this agrees very well with the predicted curve.

References

[1] McCrum N G, Read B E and Williams G 1991 *Anelastic and Dielectric Effects in Polymeric Solids* (New York: Dover)
[2] Ferry J D 1961 *Viscoelastic Properties of Polymers* (New York: Wiley)
[3] Kolrausch R 1854 *Poggendorff's Ann. Phys.* **1** 179
[4] Williams G and Watts D C 1970 *Trans. Faraday Soc.* **66** 80
[5] Havriliak S and Negami S 1966 *J. Polym. Sci.* C **14** 99
[6] Vogel H 1921 *Phys. Z.* **22** 645
[7] Tammann G and Hesse W 1926 *Z. Anorg. Allg. Chem.* **156** 245
[8] Fulcher G S 1925 *J. Am. Ceram. Soc.* **8** 339
[9] Ishida Y, Yamafuji K, Ito H and Takayanagi M 1962 *Kolloid-Z. Z. Polym.* **184** 97
[10] Ishida Y, Amano O and Takayanagi M 1960 *Kolloid-Z.* **172** 129
[11] Hayakawa R, Nishi T, Arisawa K and Wada Y 1967 *J. Polym. Sci.* A-2 **5** 165
[12] Saito S and Nakayima T 1959 *J. Appl. Polym. Sci.* **2** 93
[13] Nakajima T and Saito S 1958 *J. Polym. Sci.* **31** 423

[14] Scott A H, Scheiber D J, Curtis A J, Lauritzen J I and Hoffman J D 1962 *J. Res. NBS* A **66** 269
[15] Curtis A J 1961 *J. Res. NBS* A **65** 185
[16] Baker W O and Yager W A 1942 *J. Am. Chem. Soc.* **64** 2171
[17] Sjögren L 1991 *J. Phys.: Condens. Matter* **3** 5023
[18] Flach S, Götze W and Sjögren L 1992 *Z. Phys.* B **87** 29
[19] Halalay I 1996 *J. Phys.: Condens. Matter* **8** 6157
[20] Eliasson H, Mellander B-E and Sjögren L 1998 *J. Non-Cryst. Solids* **235–237** 101
[21] Hansen J-P and McDonald I R 1986 *Theory of Simple Liquids* 2nd edn (London: Academic)
[22] Kawasaki K 1966 *Phys. Rev* **150** 291
[23] Götze W 1991 *Liquids, Freezing and Glass Transition* ed J-P Hansen, D Levesque and J Zinn-Justin (Amsterdam: North-Holland)
[24] Gilmore R 1981 *Catastrophe Theory for Scientists and Engineers* (New York: Wiley)
[25] Arnol'd V I 1986 *Catastrophe Theory* 2nd edn (Berlin: Springer)
[26] Götze W and Sjögren L 1992 *Rep. Prog. Phys.* **55** 241
[27] See the review articles in *Transport Theory Stat. Phys.* 1995 **24**
[28] Götze W and Sjögren L 1989 *J. Phys.: Condens. Matter* **1** 4203